J Appl Electrochem (2010) 40:1455–1460
DOI 10.1007/s10800-010-0123-9

ORIGINAL PAPER

Anodic electrodeposition of ZnO onto p-Si substrates assisted by light irradiation

K. Laurent · D. P. Yu · Y. Leprince-Wang

Received: 26 August 2009 / Accepted: 27 March 2010 / Published online: 11 April 2010

Abstract ZnO was electrodeposited on *p*-type silicon substrates with the assistance of light irradiation in order to allow the presence of electrons at the interface of the semi-conductor/electrolyte. The electrodeposition was performed at −0.9 V versus Standard Hydrogen Electrode (SHE). Scanning electron analysis revealed that the ZnO deposit consisted of small islands of ZnO randomly dispersed on the *p*-Si surface. The small islands are in the order of the micron size, and cover ~37% of the whole surface after 4 min of deposition. The characteristic E_2 vibration mode in the Raman spectroscopy was clearly observed from the as-deposit ZnO. Photoluminescence measurements of the deposit reveal that the near band edge emission of ZnO is ~12 times more intense than the defects emission band around 543 nm, which is attributed to the presence of interstitial oxygen, and may come from the electrodeposition process in an oxygen rich medium.

Keywords ZnO · p-Si · Electrodeposition · Raman spectroscopy · Photoluminescence

1 Introduction

ZnO is one of the most studied metal oxides. Its wide band gap ~3.36 eV and other unique optical, electrical and mechanical properties makes ZnO a good candidate in a large variety of fields such as light emitting diodes [1], piezo-electric transducers [2], gas sensors [3] and transparent oxide conductors [4]. ZnO deposition on *p*-type semi-conductor has proven to be an efficient way to obtain high quality photodiodes [5].

Among different synthesis techniques used to fabricate ZnO, such as PVD [6], CVD [7], or sol–gel [8], electrodeposition method possesses several advantages such as low cost of equipments and low temperature process. The electrodeposition was used by our group to deposit ZnO on different substrates such as gold, stainless steel, copper [9], or on heavily doped *n*-type semiconductors such as ITO [10], or *n*-Si [11]. To our knowledge, few reports deal with the electrodeposition of ZnO on a *p*-type semi-conductor, partially due to the electron blocking type of the *p*-type semi-conductor.

Here, we report on the electrodeposition of ZnO on a *p*-type silicon substrate using light irradiation. The electrodeposition process implied a reduction of an oxygen precursor at the surface of the substrate, and then the use of *n*-type semiconductors or a metallic substrate. Light irradiation is then used to enable the presence of electrons at the interface electrode/electrolyte and then allow the growth of ZnO on a *p*-type semiconductor [12]. The ZnO grown using light irradiation is of a high quality and showing low defects signal in PL experiments. The direct electrodeposition of ZnO on *p*-type semiconductors will be of great interest especially for the fabrication of photoactive ZnO devices.

2 Experimental details

The electrolytic solution used for the electrodeposition of ZnO was composed of 0.1 M of KCl as supporting

K. Laurent · Y. Leprince-Wang (✉)
Laboratoire de Physique des Matériaux Divisés et Interfaces (LPMDI), CNRS-FRE 3300, Université Paris-Est, 5 Bd. Descartes, 77454 Marne la Vallée Cedex 2, France
e-mail: yamin.leprince@univ-mlv.fr

D. P. Yu
School of Physics, Electron Microscopy Laboratory, and State Key Laboratory for Mesoscopic Physics, Peking University, Beijing 100871, People's Republic of China

electrolyte, 5 mM $ZnCl_2$ as the source of zinc, and 2.5 mM of H_2O_2 as the source of hydroxide ions (all reagents were purchased from ACROS). The electrochemical bath obtained is quasi-neutral, its pH value being ~6.5. The solution was prepared with ultra pure water (>18 MΩ) from a Millipore system, and the temperature of the bath was kept at 70 °C during the deposition.

Prior to the deposition, polarization experiments have been performed using a three-electrode cell with a platinum counter-electrode, a mercurial sulfate electrode [MSE, +0.642 V vs. Standard Hydrogen Electrode (SHE)] as the reference electrode and a *p*-Si substrate (B doped Si with resistivity between 0.001 and 0.005 $\Omega\,cm^{-1}$) as the working electrode. The effective area of the substrate was ~0.20 cm^2, was limited by a circular Teflon mask. A PGZ100 potentiostat–galvanostat was used to apply the electrochemical method to the electrochemical cell. Polarization experiments were performed in different solutions containing reactants used in the electrodeposition process, the scanning speed being 50 mV s^{-1} and the solvent was deionised water. Light irradiation was obtained using a 100 W tungsten lamp, which was placed just above the solution surface (~5 cm distant from the substrate). Polarization experiments helped us to choose the suitable conditions to electrodeposit ZnO. Electrodeposition is then performed using the same three-electrode cell with a *p*-Si substrate as the working electrode.

The deposit morphology was studied using an FEI QUANTA 200F environmental field emission scanning electron microscope (ESEM) operating at 10 kV accelerating voltage. Photoluminescence spectroscopy was performed at room temperature using a micro-Raman system (Renishaw Invia). A He–Cd laser working at TEM_{00} single mode at 325 nm and 30 mW output power was used as the excitation source for photoluminescence measurements. The Raman spectroscopy was conducted in the near backscattering geometry using an Ar^+ laser (515 nm) with a power of 20 mW.

3 Results and discussions

3.1 Electrodeposition

In order to optimize the ZnO electrodeposit onto *p*-Si substrates conditions, we carried out a brief electrochemical process study. The electrodeposition of ZnO through the reduction of an oxygen precursor has been widely investigated and can be described by a three-step process [13]:

First, the oxygen precursor is reduced near the electrode, in our case H_2O_2 is reduced to OH^- which begins to diffuse in the solution:

$$H_2O_2 + 2e^- \rightarrow 2OH^- \quad E_0 = -0.33 \text{ V versus SHE}$$

Second, Zn^{2+} ions in the solution combine with the OH^- and form $Zn(OH)_2$:

$$Zn^{2+} + 2OH^- \rightarrow Zn(OH)_2$$

Third, the $Zn(OH)_2$ decomposes into ZnO through a dehydration reaction. Its equilibrium can be shifted towards the formation of ZnO by increasing the temperature:

$$Zn(OH)_2 \rightarrow ZnO + H_2O$$

Polarisation curves of different electrolytic solutions are shown in Fig. 1. The first curve (Fig. 1a) shows the reduction

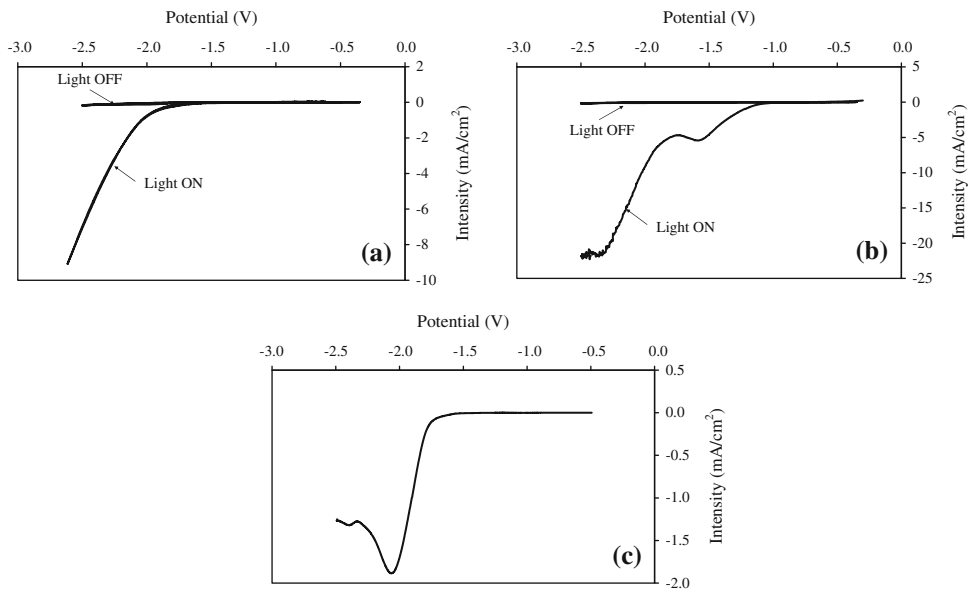

Fig. 1 Polarization curves of a solution containing: 0.1 M KCl (**a**), 5 mM of H_2O_2 and 0.1 M of KCl (**b**), and 0.1 M KCl and 5 mM $ZnCl_2$ (**c**), respectively, in deionised water. The substrate is *p*-type silicon, the potential is set versus SHE, and the temperature is 70 °C

of our supporting electrolyte, which is H_2O. It can be seen that when the light is turned off, no electrochemical reaction occurs and the current density passing through the solution is really low whatever the potential applied is. This is due to the *p*-type nature of the substrate in use. When the light is turned on, a rapid increase of the current density is observed for a potential values lower than −1.0 V. The increase of the current density is attributed to the reduction of H_2O into H_2.

The second curve (Fig. 1b) shows the polarisation curves of the electrolytic solution containing the oxygen precursor H_2O_2. When the light is turned off, no electrochemical reaction is detected, and this is due to the *p*-type nature of the Si substrate. When the light is turned on, the current density increased rapidly for a potential lower than −0.5 V, which means that the reduction of the precursor is engaged at this potential. A plateau is reached around −1.0 V, which corresponds to the saturation current due to the diffusion of active species (H_2O_2) towards the electrode. For potentials lower than −1.2 V, the current density increased rapidly due to the reduction of H_2O into H_2.

Finally, the third curve describes the reduction process of Zn^{2+} into Zn onto *p*-Si. It would be noted that the reduction potential of Zn^{2+} is very important in order to limit the presence of metallic Zn in the final deposit. In the case of zinc reduction, the curve displayed on Fig. 1c shows that the reduction wave is engaged at −1.1 V. In order to avoid both the electrodeposition of zinc and the reduction of H_2O into H_2, we have chosen to perform the electrodeposition at −0.9 V.

The curve a in the Fig. 2 shows the current passing through the solution when a potential of −0.9 V is applied and the lamp is kept off during 20 min. The observed current is very low around −0.2 mA cm^{-2} and no ZnO deposition is observed even if the deposition time is increased up to 1 h. The nature of the electrode which is a *p*-type semiconductor blocks the transfer of electrons from the electrode to the solution, resulting in a very low current density and no electrochemical reaction at the electrode.

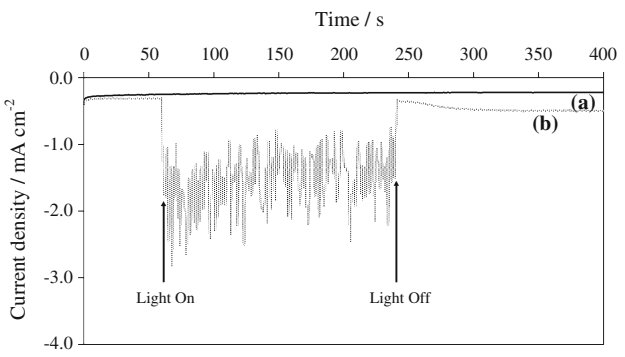

Fig. 2 Current density curves obtained when a potential of −0.9 V is applied during 30 min: without irradiation (**a**), and with 3 min irradiation (**b**)

The curve b on the Fig. 2 shows the results of an experiment on which we switch on the lamp after 1 min and then let the light on during 3 min before switch off. As soon as we turn the light on, we observed a significant increase of the current, indicating that an electrochemical reaction occurred at the interface. In facts, the light ensures the presence of charges carriers (electrons) which are able to reduce the H_2O_2 into OH^-. This allows the reaction to occur. The current passing through the solution does not recover its initial value when the light is switched off after 3 min of irradiation, suggesting that the reaction still occurs even when the light is turned off. This can be explained by the fact that the ZnO deposit is an *n*-type semiconductor and thus, electrons can be conducted then towards the interface within the electrolyte.

3.2 SEM analysis

SEM images of the electrodeposited ZnO on *p*-Si substrates are shown on Fig. 3. These images reveal ZnO deposit morphology for different reaction times (1–4 min). We can first see that the growth of ZnO is heterogeneous, resulting in the presence of micro-sized particles with a diameter of ∼2 μm. The micro-sized particles cover ∼17% of the entire surface after 1 min of deposition, and ∼37% after 4 min. Even if the electrodeposition curves suggest that the growth continues after the light is switched off, the SEM images do not show any major change, which can be explained by the slow growth of ZnO without irradiation. The microparticles form small islands growing with irradiation time while their surface is very granular.

The poor coverage of the silicon surface by ZnO is not totally understood and it may be due to the one of those three reasons: the lattice mismatch between silicon and zinc oxide, the nucleation on the silicon surface, and/or the electrodeposition mechanism. ZnO presents a hexagonal compact structure with cell parameters $a = 0.348$ nm and $c = 0.521$ nm, while silicon exhibit a diamond structure with a cell parameter $a = 0.543$ nm. The lattice mismatch is a well-known reason for heterogeneous growth on a substrate. Another possible explanation of the poor coverage of the silicon surface is the low concentration of nucleation point on the silicon surface which can inhibit the initiation of the growth on silicon surface. The electrodeposition mechanism can also explain the heterogeneous growth on the silicon surface. During the electrodeposition process, hydroxyls ions are produced near the silicon electrode, then hydroxyls can diffuse in the solution and then initiate the formation of $Zn(OH)_2$ in the solution and not on the electrode which can prevent further growth on the substrate.

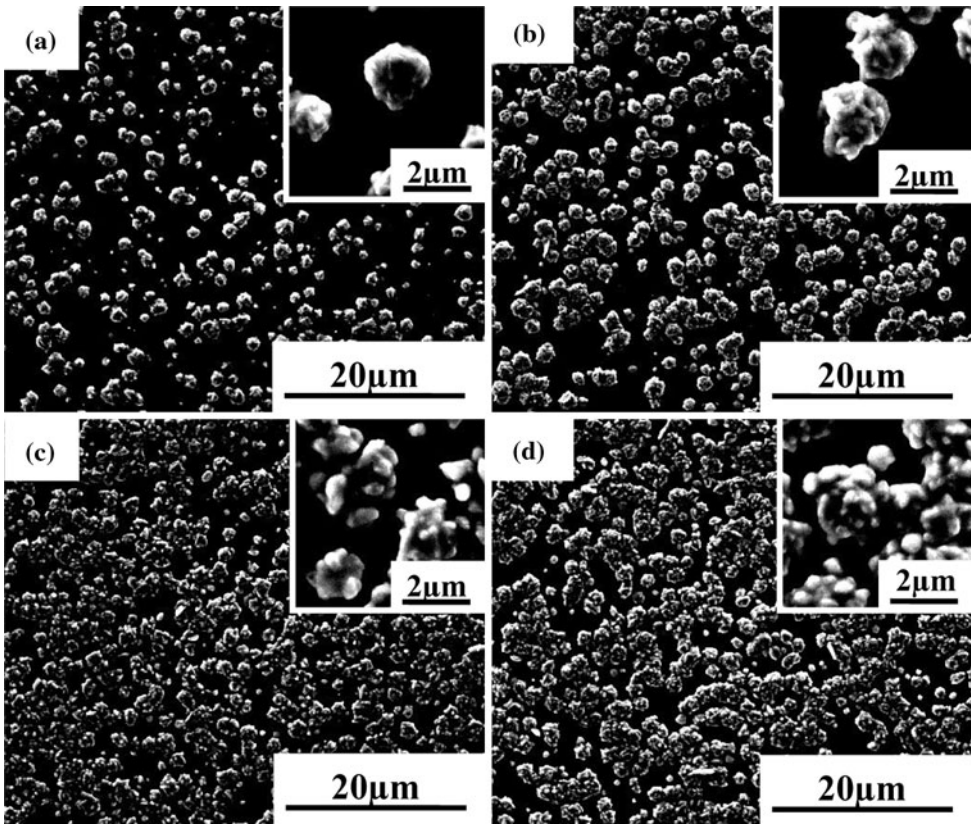

Fig. 3 SEM images of the ZnO deposited on silicon surfaces during 1 min (**a**), 2 min (**b**), 3 min (**c**) and 4 min (**d**) at a constant potential of −0.9 V (vs. SHE) under irradiation

3.3 Raman spectroscopy

Raman spectroscopy was performed on the electrodeposited ZnO in order to study the structural properties. Figure 4 shows the Raman spectra of three different deposits with increasing deposition time. As we can see from the Raman spectra, the vibration modes of the silicon substrate are very intense and cover a broad band between 500 and 550 cm^{-1}. The vibration modes corresponding to the ZnO deposits are described by group theory applied to the symmetry of ZnO crystal (C_{6v}^4). The optical phonons at the Γ point of the Brillouin zone have the symmetry $A_1 + E_1 + 2E_2 + 2B_1$, containing two Raman inactive B_1 modes. The E_1 and A_1 modes are polar modes and they will split into two different modes: longitudinal optical (LO) and transversal optical (TO) components.

In the Raman spectroscopy spectra, the peaks corresponding to the ZnO are highly covered by the response of the silicon substrate signal. Nevertheless, we observed a distinct mode $\sim$437 cm^{-1} which can be attributed to the vibration mode E_2 of ZnO [14]. In fact, by increasing deposition time, we observed that the mode at 437 cm^{-1} increased in intensity. Another mode $\sim$612 cm^{-1} is also observed. This mode can be attributed to silicon substrate, as no reference can be found about a vibration mode for ZnO $\sim$612 cm^{-1} and no peak intensity changing is observed by increasing deposition time.

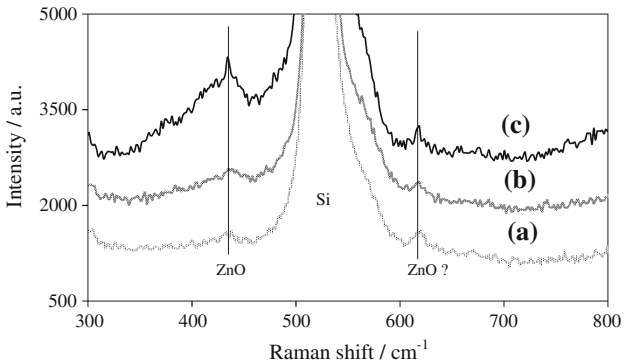

Fig. 4 Raman spectra of the ZnO electrodeposited during 1 min (**a**), 2 min (**b**), and 3 min (**c**)

3.4 Photoluminescence measurements

Photoluminescence (PL) spectroscopy measurements were conducted at room temperature in order to study the optical properties of the electrodeposited ZnO on *p*-Si. The PL spectrum of the 3 min electrodeposited ZnO on *p*-Si is shown on Fig. 5. Every ZnO deposit shows similar PL spectrum with different peak intensities according to deposition time. From the PL spectrum, we first observed a broad emission band between 330 and 400 nm, and a very weak emission band between 475 and 625 nm. The emission band observed between 330 and 400 nm is consistent of the near band edge emission from the ZnO which is

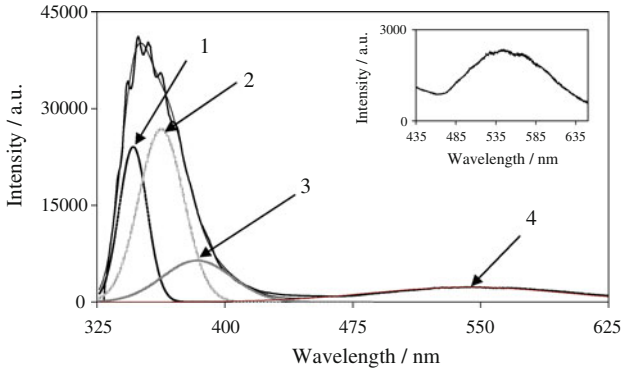

Fig. 5 PL spectrum of the ZnO electrodeposited during 3 min irradiation, and its fit through multiple Gaussian curves

Table 1 List of PL emission peaks observed on the PL spectrum of the electrodeposited ZnO on *p*-Si

Peak number	Wavelength (nm)	Energy (eV)
1	346	3.59
2	362	3.43
3	383	3.24
4	543	2.29

∼368 nm [14]. As the observed band is asymmetric, we tried to deconvolute it into several fine structures. Through multiple Gaussian fit we obtained the deconvolution of the entire spectrum and the results are listed in Table 1. The emission band observed in the UV region is composed of three different peaks centred at 346, 362 and 382 nm. The first emission peak is centred well above the band gap emission of ZnO [14], and can neither be attributed to the Burstein-Moss effect [15] nor to the quantum confinement as the grain size is larger than the Bohr radius of the ZnO [16]. The peak centred at 346 nm is then attributed to the $Zn(OH)_2$ which was not dehydrated in the deposition process. This observation is correlated to the results we previously obtained on the deposition of ZnO on metallic substrates [9]. The PL emission ∼362 nm is attributed to the direct recombination of the excitons in ZnO, which is blue shifted regarding the literature of the ZnO [14], and this effect is assumed to be the result of the presence of defects which induced a Burstein-Moss effect on the emission. Finally, the third peak observed at ∼383 nm is attributed to the presence of defects in the ZnO structure and is correlated to the so-called Urbach's Tail [17].

The PL spectra of the as-grown ZnO on *p*-Si also show oscillations in intensity near band edge emission. Similar oscillations have already been observed in the case of porous SiO_2 [18] and porous alumina [19], and have been used to extract porosity or refractive index from those materials. These oscillations originate from the interferences of the emitted light during the PL experiments as described in our previous work [9].

The observed emission in visible region is broadened between 475 and 625 nm. Through multiple Gaussian fittings, the centre of the peak appeared to be ∼543 nm. The attribution of the visible emission to defects in the structure of ZnO is still controversial. A majority of the scientific community defined three types of structural defects (oxygen vacancies, zinc interstitial, oxygen interstitial [14]) which are responsible for the three different visible emissions observed in ZnO. The inset in the Fig. 5 demonstrates a zoom on the visible region where the visible emission is observed. The band is centred on 543 nm, and can be attributed to the structural defects in ZnO. The aspect ratio between the UV and the visible emission bands is very high; revealing a low concentration of defects and high crystalline quality of the as-grown electrodeposited ZnO.

4 Conclusions

ZnO has been electrodeposited on a *p*-type substrate (*p*-Si) using an assistance of light irradiation. The deposit constituted small particles of ZnO randomly dispersed onto the silicon surface. After only 4 min of electrodeposition, ∼37% of the whole surface is covered by ZnO. When a longer irradiation is used, the micro particles appear more granular. Raman spectroscopy confirmed the presence of ZnO even if the signal is partially covered by the substrate response. Photoluminescence spectroscopy shown that the as-deposited ZnO is of a very good quality. Indeed, the visible region exhibits low defect emission, while band edge emission is very intensive (with a ratio up to 12 times).

References

1. Lee SY, Shim ES, Kang HS, Pang SS, Kang JS (2005) Thin Solid Films 473:31
2. Chen JJ, Zeng F, Li DM, Niu JB, Pan F (2005) Thin Solid Films 485:257
3. Hsueh TJ, Chang SJ, Hsu CL, Lin YR, Chen IC (2007) Appl Phys Lett 91:053111
4. Muller J, Rech B, Springer J, Vanecek M (2004) Sol Energy 77:917
5. Lee JY, Choi YS, Kim JH, Park MO, Im S (2002) Thin Solid Films 403:553
6. Zhou Y, Kelly PJ, Postill A, Abu-Zeid O, Alnajjar AA (2004) Thin Solid Films 447:33
7. Lu JG, Kawaharamura T, Nishinaka H, Kamada Y, Ohshima T, Fujita S (2007) J Cryst Growth 299:1
8. Shao ZB, Wang CY, Geng SD, Sun XD, Geng SJ (2006) J Mater Process Tech 178:247
9. Laurent K, Wang BQ, Yu DP, Leprince-Wang Y (2008) Thin Solid Films 517:617
10. Gu CD, Li J, Lian JS, Zheng GQ (2007) Appl Surf Sci 253:7011

11. Dalchiele EA, Giorgi P, Marotti RE, Martin F, Ramos-Barrado JR, Ayouci R, Leinen D (2001) Sol Energ Mat Sol C 70:245
12. Rappich J, Fahoume M (2005) Thin Solid Films 487:157
13. Th Pauporte, Lincot D (2001) J Electroanal Chem 517:54
14. Özgür Ü, Alivov YI, Liu C, Teke A, Reshchikov MA, Doğan S, Avrutin V, Cho SJ, Morkoç H (2005) J Appl Phys 98:041301
15. Marotti RE, Guerra DN, Bello C, Machado G, Dalchiele EA (2004) Sol Energ Mat Sol C 82:85
16. Schoonman J (2003) Solid State Ionics 157:319
17. Ong HC, Du GT (2004) J Cryst Growth 265:265471
18. Huang K, Pu L, Shi Y, Han P, Zhang R, Zheng YD (2006) Appl Phys Lett 89:201118
19. Von Behren J, Tsybeskov L, Fauchet PM (1995) Appl Phys Lett 66:1662